Supporting Information for

Assessing coastal plumes in a region of multiple discharges: the U.S.–Mexico border

Sung Yong Kim*, Eric Terrill, and Bruce Cornuelle

Scripps Institution of Oceanography

9500 Gilman Dr., La Jolla, CA 92093

*To whom correspondence should be addressed. E-mail: syongkim@mpl.ucsd.edu

Complement description of observations

Water quality sampling

The distribution of the bacterial levels along the shoreline is examined with the annual mean at each station over three FIB levels for ten years (January 1996 to March 2007): *Total Coliform* (TC, Figure SI–S1a), *Fecal Coliform* (FC, Figure SI–S1b), and *Enterococcus* (ENT, Figure SI–S1c). The horizontal axis is not scaled with the physical distance between stations to avoid the overlapped plots. The highest FIB concentration is at C6 station closest to the TJR mouth. The FIB levels in the southern area of the TJR are slightly higher than the northern side. The relatively higher level of TC near the Punta Bandera discharge at Los Buenos creek is observed (*S1*).

Rainfall in San Diego and Tijuana River flow

The river flow due to rainfall shows a time-lagged response: in the initial stage of rainfall the river flow is nearly proportional to it, then once rainfall reaches its peak, the river flow is almost steady and decreases slowly (Figure SI–S2).

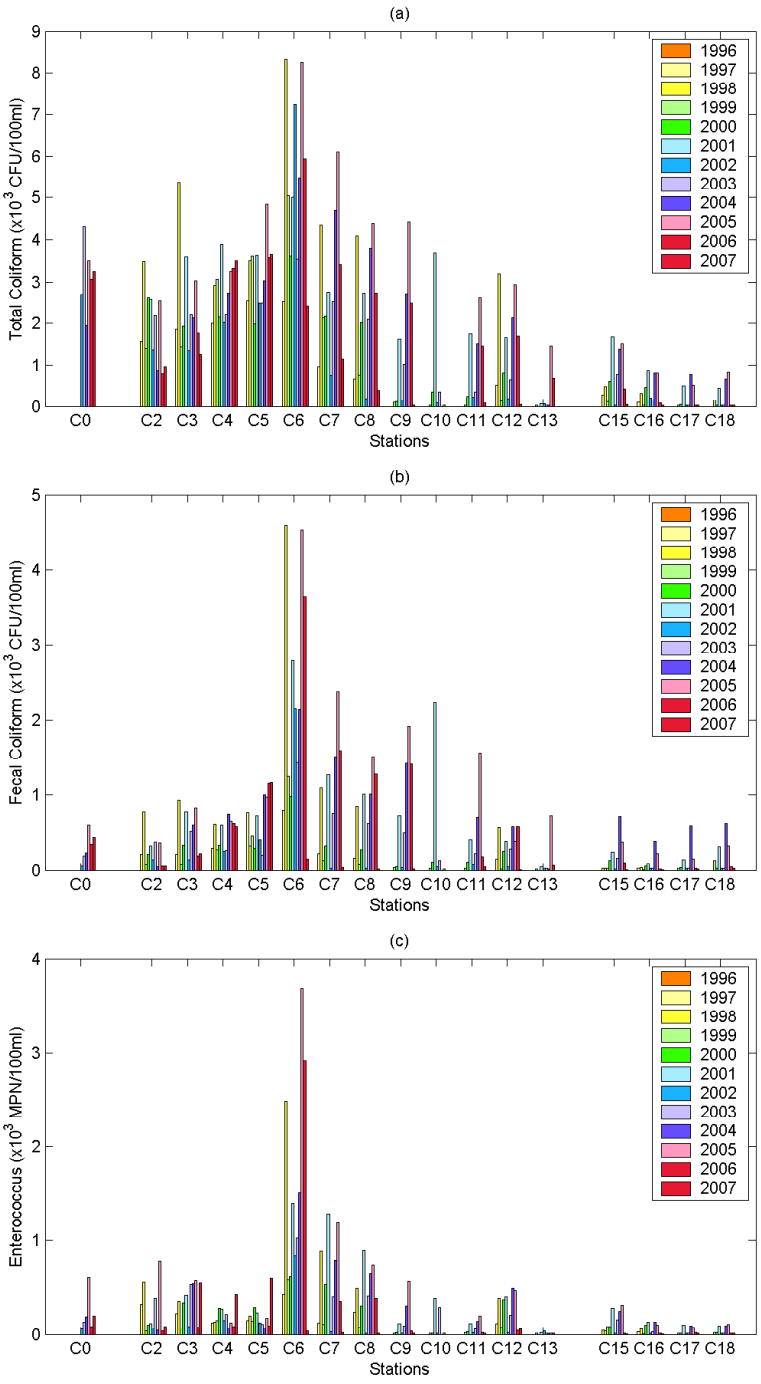

Figure SI–S1: Annual mean of the FIB sampling data (January 1996 – March 2007). (a) *Total Coliform* (TC). (b) *Fecal Coliform* (FC). (c) *Enterococcus* (ENT).

Table SI–S1: A unified water quality sampling stations along the southern San Diego coastline and the number of sampling data for about eleven years (January 1996 – March 2007). The water quality data at C1 and C14 stations are reported from historical records, but they are not included in the analysis due to their sparse observations and the lack of station information.

ID	City ID	County ID	Station name	The number of samplings
C0	S0	BC-010	Playa Blanca	232
C2	S2	BC-020	El Vigia	507
C3	S3	BC-030	Playas de Tijuana	507
C4	S4	IB-010	Border Fence	1252
C5	S10	IB-020	Monument Road	1257
C6	S5	IB-030	Tijuana River Mouth	1416
C7	S11	IB-040	3/4 miles North of Tijuana River	1342
C8	S6	IB-050	End of Seacoast Drive	1447
C9		EH-010	Cortez Avenue	380
C10		EH-020	Imperial Beach Boulevard	78
C11		EH-030	Imperial Beach Pier	604
C12	S12	IB-060	Carnation Avenue	1339
C13		EH-041	Camp Surf Jetty	231
C15	S8/D2	IB-070	Silver Strand Beach	1385
C16	S9/D3	IB-080	Avenida del Sol	2042
C17		EH-050	Loma Avenue	859
C18		EH-060	Navy Fence	853

Climatological data

The NPDES permit of the SBO discharge includes monthly vertical sampling of temperature, salinity, density, and chlorophyll-a. The data are obtained using a conductivity, temperature, depth (CTD) sensor, and stations are vessel occupied both in the nearshore and offshore within 15 km from the coast including dense sampling near the SBO. Typical sampling stations are shown as dots in Figure SI–S3a and Figure SI–S3b, and they are occupied in a 2–4 day window for sampling.

Examples of the TJR plume and the SBO plume detected in the salinity data from the CTD stations are shown as the linearly interpolated surface (Figure SI–S3a) and bottom (Figure SI–S3b) maps and vertical sections in the cross-shore direction (Figure SI–S3c and Figure SI–S3d). The cross-shore sections of salinity (Figure SI–S3c and Figure SI–S3d) use the salinity data within a rectangular box in Figure SI–S3a and Figure SI–S3b. During a heavy rain in January 2005, a lower salinity front (less than 32.6 psu) was observed in front of the TJR mouth and reached near

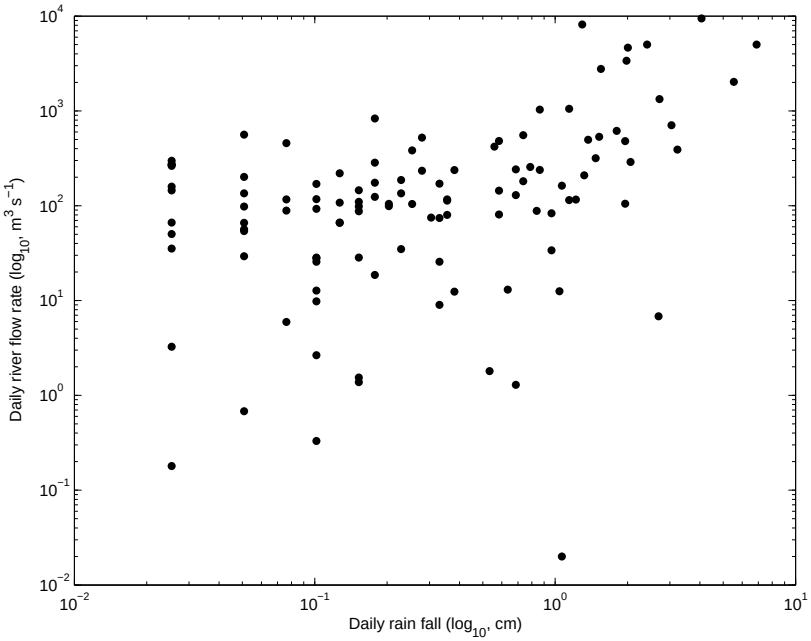

Figure SI–S2: The scatter plot (log scale) of the daily rainfall at SAN and the daily TJR flow rate (2003 – 2007).

12 km from the coast with a film in the 1–2 m upper layer (Figure SI–S3a and Figure SI–S3c). This surface advected jet due to buoyancy difference is a typical flow pattern of the river plume in the coastal region (*S2*, *S3*, *S4*). On December 2003, the lower salinity water (less than 32.9 psu) near the outfall was trapped within 20 m of the bottom and spread in the alongshore direction.

Remote sensing data

Satellite images of total suspended matter (TSM) and chlorophyll-a (Chl-a) in the study area are used for qualitative verification of the offshore surface transport. The satellite IRS-P4 (Indian Remote Sensing Satellite or OCEANSAT-1) carries two sensors MSMR (Multichannel Sacnning Microwave Radiometer) for data collection on SST, wind speed, and atmospheric water vapour and OCM (Ocean Color Monitor) for data on atmospheric aerosols, suspended sediments, chlorophyll concentration, and reports the identical coverage of a given area every 48 hours (*S5*, *S6*). During a storm event on January 2–6 of 2005 the higher density TSM and Chl-a were observed as a

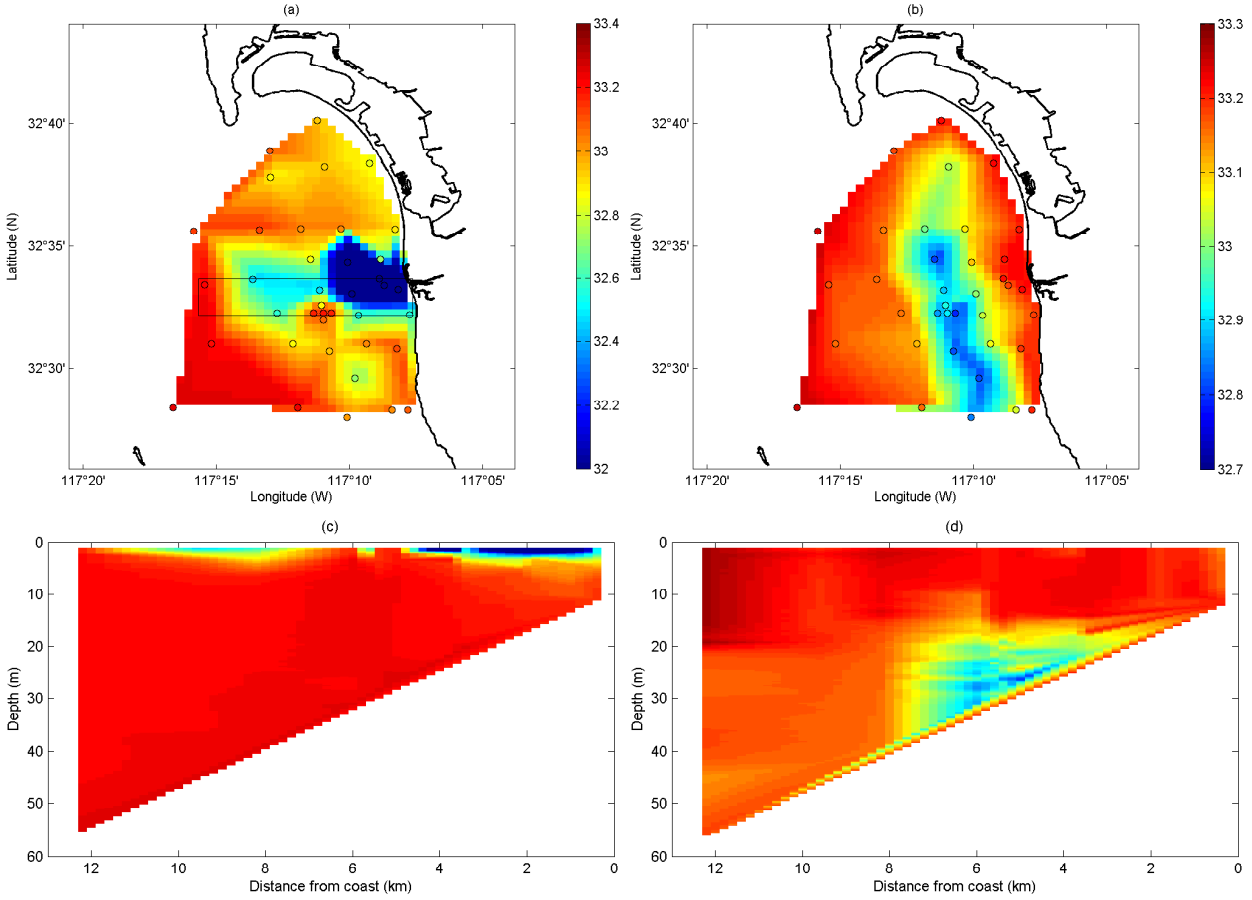

Figure SI–S3: Linearly interpolated salinity (psu) surface/bottom maps and vertical section in the crossshore direction. (a) and (c): Surface map and vertical section of salinity during the one of heavy rain events on January 2–6, 2005. (b) and (d): Bottom map and vertical section of salinity on December 16, 2003. The vertical sections of salinity [(c) and (d)] use the salinity data within the rectangular box on (a) and (b).

stretched tongue or a jet (Figure SI–S4a and Figure SI–S4b, respectively) as the salinity surface map in Figure SI–S3a.

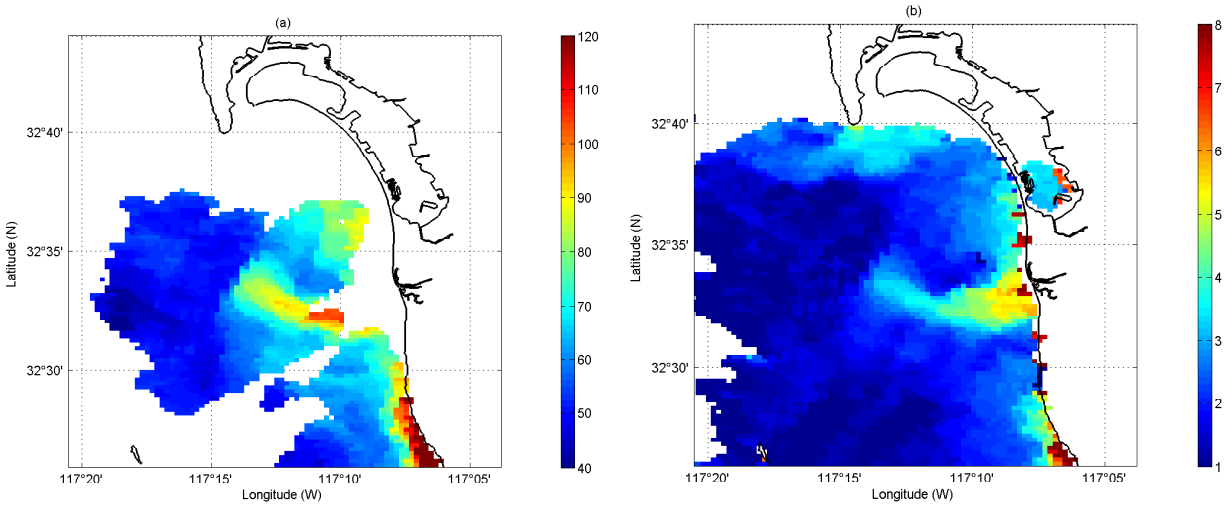

Figure SI–S4: Ocean satellite images: (a) Total suspend matters ($\mathrm{mg\,L^{-1}}$) and (b) Chlorophyll-a ($\mathrm{mg\,m^{-3}}$) during a heavy rain event on January 6 1939, 2005 (GMT).

Surface currents

The dominant variance in the surface currents in this region is the low frequency band (less than 0.4 cpd) and cuspate tidal peaks at the diurnal (K1) and semidiurnal (M2) frequencies superposed on a red spectrum [$S(\omega) \propto \omega^{-2}$]. Since the time integration of the surface currents is a low-pass filter [$S(\omega) \propto \omega^{-4}$], the Lagrangian surface transport should be dominantly driven by the subinertial variability. The magnitude of the low frequency surface currents is approximately 10 $\mathrm{cm\,s^{-1}}$, so the Lagrangian surface transport is expected to exit the study domain (40×40 $\mathrm{km^2}$) within about 5 days. A typical surface current map is shown in Figure SI–S5.

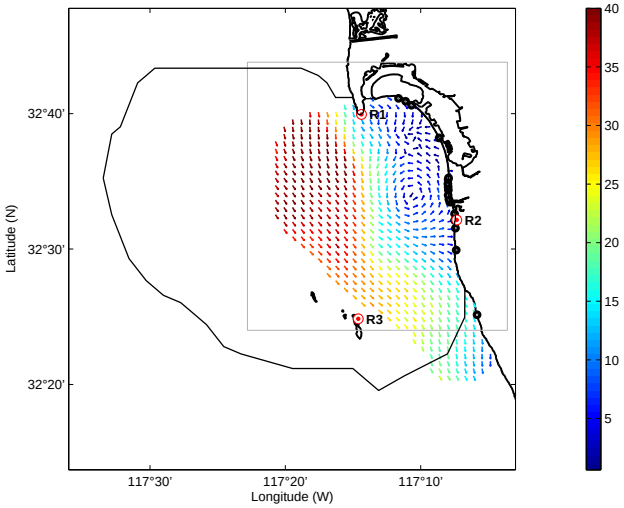

Figure SI–S5: An example of the objectively mapped surface current field [May 31 0000Z, 2003 (GMT)] is presented with the current speed color-coded ($\mathrm{cm\,s^{-1}}$). The effective spatial coverage area where the HF radars (R1, R2, and R3) observed is indicated with black curve (at least 70% data availability over four-year observations), and a gray square box denotes the study area in the paper.

Regional discharges

Coastline discharge: Tijuana River

The rainfall in southern San Diego and the TJR outflow are concentrated during the winter season (Figure 2b and Figure 2c), and FIB exceedance at the TJR mouth (C6 station) is 93% coherent with the existence of the TJR flow. Due to the high correlation of high FIB with the TJR flow, we use flow conditions as the trigger for when to track water parcels from the TJR source.

Submerged discharge: South Bay International Wastewater Treatment Plant (SBIWTP)

The dynamics of the plume is controlled by the outfall design and density structure with depth in the near-field and the ocean variabilities in the far-field (e.g., winds, tides, alongshore pressure gradient, and internal waves). The U.S. EPA Roberts-Snyder-Baumgartner (RSB) plume model (*S7*, *S8*, *S9*) has been used to predict the height of the plume and the potential for active surfacing

within the near-field. The RSB model is based on the assumptions of linear stratification between neighboring vertical observations, uniform currents, straight diffusers, and Gaussian spreading of plume water concentrations at the end of the near-field (*S8*, *S9*, *S10*). The plume height (H) is parameterized in the RSB model as

$$H = H(\rho(z), \mathbf{u}(\mathbf{x}, z_0), q; n, D, \Delta d, z_0, \theta_0, \rho_q), \tag{SI–S1}$$

where $\rho(z)$, $\mathbf{u}(\mathbf{x}, z_0)$, and q denote the ambient density profile, the current at the plume depth, and the amount of outfall flow ($\mathrm{m^3\,s^{-1}}$), respectively. The SBO plume specifications and the RSB model outputs are described in Table SI–S2a and Table SI–S2b, respectively. The behavior of the plume in the near-field is estimated with the RSB model, and the transport in the far-field of the surfacing plume water is tracked with Lagrangian trajectory analysis of hourly surface current maps, which will be discussed in the following section. The surfacing of the SBO plume water is used for triggering when to tack transport.

Table SI–S2: (a) Inputs and (b) outputs of the RSB model to examine the near-field behavior of the SBO (*S7*, *S11*, *S12*).

(a)

Model inputs	Input data
Number of ports, n	60
Port diameter, D (m)	5
Port spacing, Δd (m)	3.66
Discharge depth, z_0 (m)	28
Diffuser orientation, θ_0 (degrees, clockwise @ N)	11.7
Effluent density, ρ_q ($\mathrm{g\,cm^{-3}}$)	0.997
Discharge amounts, q (MGD)	20
Number of points in density profile	13

(b)

Model outputs
Minimum dilution at the end of near-field, S_n
Rise height from the bottom, z_e (m)
Thickness of plume, h_e (m)
Height to level of near-field dilution, z_m (m)
Length of the near-field, x_n (m)

The SBO has improved the impaired coastal water quality in southern San Diego since 1999

(*S1*, *S13*). However, the improvements during dry and wet seasons needs to be investigated with continuous observations. (*S14*, *S15*) found that the density stratification is closely related to the temperature rather than salinity in the Southern California Bight, which allows the density profile to be calculated from vertical temperature profile (*S16*, *S17*). Due to limited observations of the current profile, the bottom current is assumed as Gaussian variables using the mean and RMS of the ADCP observations at that location, which are 5.5 and 2.3 cm s^{-1}, respectively. The estimated plume rise height is found to be less sensitive to the bottom current.

The predicted ceiling depth (z_e) is highly dependent on the stratification: the strong stratification in summer traps the plume beneath the thermocline, and the weak stratification in winter allows the plume to surface. The RSB model outputs show the approximately one hour time lag between uplifts in isotherms and the predicted ceiling depth.

The surfacing of the SBO plume takes place $\sim$25% over a year. Excluding the surfacing events, the plume ceiling is on average 9.3 m (mean depth) with 3.5 m (RMS). The vertical temperature differences between top and bottom depths during surfacing and non-surfacing events are less than 1 degree and 5–6 degrees, respectively. The monthly histogram of the ceiling depth shows the frequent surfacing during winter and intermittent breakdown of the stratification during summer, which can explain the anomaly in August. The four years of temperature data (April 2003 – March 2007) have some gaps which can bias the seasonal statistics: the missing observations are 8 and 2 months for summer and winter seasons during four years, respectively, and those are 33 and 8.3% of each season.

Coastline discharge: Punta Bandera discharge

The Los Buenos Creek continuously discharges 0.97–1.46 $m^3\,s^{-1}$ of minimally treated sewage effluent from the San Antonio de Los Buenos Sewage Treatment Facility near Tijuana (*S18*, *S19*). (*S19*) reported the higher bacteria concentration near the PBD due to the treatment facility, and discussed the impaired water quality at the U.S.–Mexico border dominantly resulted from the TJR than the PBD. Since it is a continuous discharge, not conditional trigger for the source is necessary.

Notes on exposure kernels and ROC analysis

The bin size of exposure kernels is determined by the typical current variance, the diffusion term used in the random walk model (i.e., uncertainty of surface current measurements in this paper), and the scale to resolve with the probability map. The smaller bin size can capture the exposure kernels with smaller scale features. The transported distance of particles due to the diffusion and background current field should be comparable with the bin size.

The number of particles within the nearcoast cell is counted using the projection to the piece-wise coastline. The coefficients (a, b, and c) are estimated from the longitude (x) and latitude (y) of the piece-wise coastline and the distance (d) from the one end.

$$d = ax + by + c \tag{SI–S2}$$

$$\mathbf{d} = \mathbf{G}\mathbf{m} \tag{SI–S3}$$

where $\mathbf{m} = [a\ b\ c]^{\dagger}$. The estimated coefficients ($\hat{\mathbf{m}}$),

$$\hat{\mathbf{m}} = \left(\mathbf{G}^{\dagger}\mathbf{G}\right)^{-1}\mathbf{G}^{\dagger}\mathbf{d}, \tag{SI–S4}$$

is used to project the each location of the particles within the nearcoast cell into the one-dimensional axis (distance from the one end). This ad-hoc one-dimensional projection can be valid within the limited crossshore direction (e.g., the nearcoast cell).

The idealized histograms of the number of particles within the nearcoast cell for $\mathscr{C}$ and $\mathscr{D}$ conditions are shown in Figure SI–S6. α and β are evaluated as a function of threshold (λ). A model with no skill has completely overlapping clean and contaminated histograms. However, a perfect model would have complete separation between two histograms.

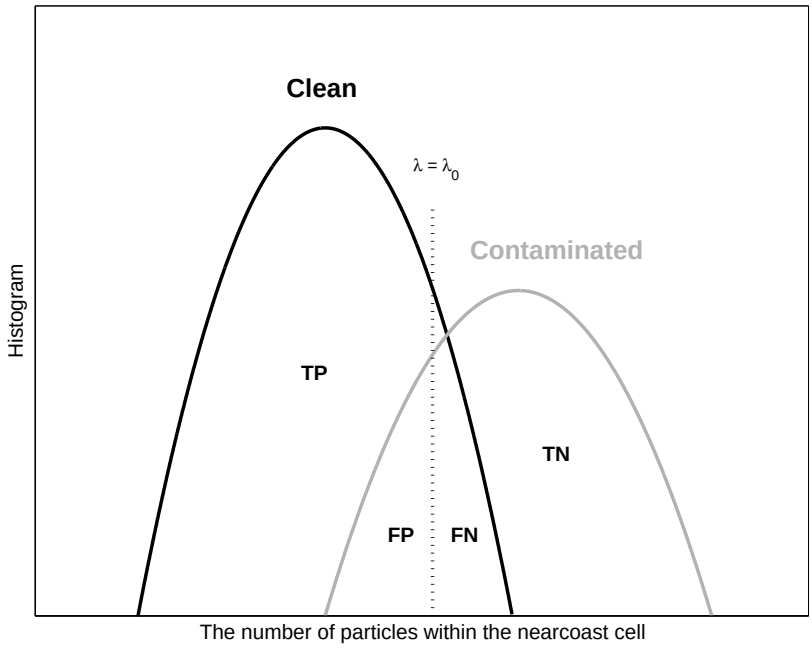

Figure SI–S6: Variables in the Receiver Operating Characteristic (ROC) analysis are a function of threshold (λ) : true-positive (TP), false-negative (FN), false-positive (FP), and true-negative (TN).

References for Supporting Information

(S1) James, D.; Groce, A. Water quality in the South Bay region off San Diego, Southern California spatial and temporal trends in bacteria levels. *California and the World Ocean 2006*, 2006.

(S2) Yankosvky, A. E.; Chapman, D. C. A simple theory for the fate of buoyant coastal discharge. *J. Phys. Oceanogr.* **1997**, *27*, 1386–1401.

(S3) MacDonald, D. G.; Geyer, W. R. Hydraulic Control of a Highly Stratified Estuarine Front. *J. Phys. Oceanogr.* **2005**, *35*, 374–387.

(S4) McCabe, R. M.; Hickey, B. M.; MacCready, P. Observational estimates of entrainment and vertical salt flux in the interior of a spreading river plume. *J. Geophys. Res.* **2008**, *113*, C08027, doi:10.1029/2007JC004361.

(S5) Space Applications Centre (ISRO), *Indian Remote Sensing Satellite IRS-P4 utilisation plan*; Technical Report SAC-RSA/IRS-P4-UP/PP-02/97, 1997.

(S6) Space Applications Centre (ISRO), *Detailed Design and Analysis report on IRS-P4 Ocean colour monitor*; Technical Report SAC/IRS-P4/01/05/98, 1998.

(S7) Roberts, P. J. W.; Snyder, W. H.; Baumgartner, D. J. Ocean outfalls. I: Submerged wastefield formation. *J. Hydr. Engr. ASCE* **1989**, *115*, 1–25.

(S8) Roberts, P. J. W. Modeling Mamala Bay outfall plumes. I: Near field. *J. Hydr. Engr. ASCE* **1999**, *126*, 564–573.

(S9) Roberts, P. J. W. Modeling Mamala Bay outfall plumes. II: Far field. *J. Hydr. Engr. ASCE* **1999**, *126*, 574–583.

(S10) Frick, W. E.; Roberts, P. J. W.; Davis, L. R.; Keyes, J.; Baumgartner, D. J.; George, K. P. *Dilution models for effluent discharges (Visual Plumes)*, version 4th; Standard and Applied Science Division Office of Science and Technology, 2001.

(S11) Largier, J.; Rasmussen, L.; Carter, M.; Scearce, C. *Evaluation of the South Bay international waste-water treatment plant receiving water quality monitoring program to determine its ability to identify source(s) of recorded bacterial exceedances*; Scripps Institution of Oceanography, University of California, San Diego, Final Report, 2004.

(S12) San Diego County, *California Regional Water Quality Control Board San Diego Region, Order No. 2000-129*, City of San Diego, 2000.

(S13) Gersberg, R.; Tiedge, J.; Gottstein, D.; Altmann, S.; Watanabe, K.; Luderitz, V. Effect of the South Bay Ocean Outfall (SBOO) on ocean beach water quality near the USA-Mexico border. *Int. J. Environ. Health Res.* **2008**, *18*, 149–158.

(S14) Bratkovich, A. Aspects of the tidal variability observed on the Southern California continental shelf. *J. Phys. Oceanogr.* **1985**, *15*, 225–239.

(S15) Winant, C. D.; Bratkovich, A. W. Temperature and currents on the southern California shelf: A description of the variability. *J. Phys. Oceanogr.* **1981**, *11*, 71–86.

(S16) Millero, F. J.; Poisson, A. International one-atmosphere equation of state of seawater. *Deep Sea Res.* **1981**, *28A*, 625–629.

(S17) Fofonoff, N. P.; Millard Jr., R. C. *Algorithms for computation of fundamental properties of seawater*; UNESCO Technical Papers in Marine Science, UNESCO/SCOR/ICES/IAPSO Joint Panel on Oceanographic Table and Standards and SCR Working Group 51: Place de Fontenoy, 75700 Paris, France, 1983.

(S18) Svejkovsky, J.; Jones, B. Detection of coastal urban stormwater and sewage runoff with synthetic aperture radar satellite imagery. *Eos, Trans., Amer. Geophys. Union* **2001**, *82*, 621, 624–625, and 630.

(S19) Orozco-Borbon, M. V.; Rico-Mora, R.; Weisberg, S. B.; Noble, R. T.; Dorsey, J. H.; Leecaster, M. K.; McGee, C. D. Bacteriological water quality along the Tijuana-Ensenada, Baja Calilfornia, Mexico shoreline. *Marine Pollution Bulletin* **2006**, *52*, 1190–1196.